Theoretical Investigation of the Mechanism of the Hock Rearrangement with InCl3 as Catalyst

Agathe Fayet, Sophie Bourcier, Nicolas Casaretto, Bastien Nay, Gilles Frison

Theoretical Investigation of the Mechanism of the Hock rearrangement with $InCl_3$ as Catalyst

Agathe Fayet,[1,2] Sophie Bourcier,[3] Nicolas Casaretto,[3] Bastien Nay*,[2] and Gilles Frison*,[1]

[1] Sorbonne Université, CNRS, Laboratoire de Chimie Théorique, 75005 Paris, France

[2] Laboratoire de Synthèse Organique, Ecole Polytechnique, CNRS, ENSTA, Institut Polytechnique de Paris, 91128 Palaiseau, France

[3] Laboratoire de Chimie Moléculaire, Ecole Polytechnique, CNRS, Institut Polytechnique de Paris, Palaiseau, France

KEYWORDS. Peroxides, Oxidative cleavage, Rearrangement, Oxacycles, DFT study.

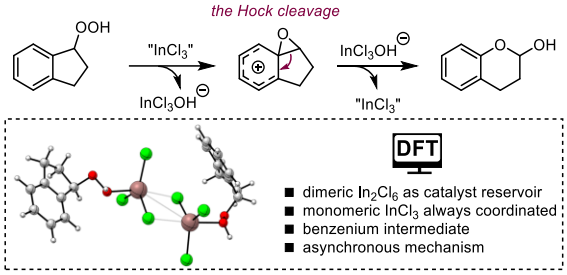

ABSTRACT: The Hock rearrangement is an acid catalyzed reaction involving organic hydroperoxides and resulting in an oxidative cleavage of adjacent C–C bonds. It has significant industrial applications, like the production of phenol (cumene process), but it remains scarcely used in organic synthesis. In addition, its detailed mechanism has never been studied. Thus, we report herein a theoretical study of the Hock rearrangement, using $InCl_3$ as a Lewis acid catalyst. The aim of this work was to fully understand the mechanism of this fundamental reaction, and to rationalize the influence of the substrate electronic properties on the reaction outcome. Furthermore, the structure of the active indium(III) catalyst interacting with the peroxide substrate was investigated, showing the superiority of a coordinated monomeric form of the Lewis acid as the active catalytic species, compared to dimeric species. However, we show that In_2Cl_6 species coordinated to the substrate are central in this catalytic cycle, serving as a reservoir of active monomeric species.

INTRODUCTION

The Hock rearrangement is the acid-catalyzed reaction of an organic hydroperoxide leading to the oxidative cleavage of a C–C bond.[1] This cleavage involves the migration of one of the adjacent carbons onto the closest oxygen of the hydroperoxide, concomitantly to the heterolytic cleavage of the O–O bond. The resulting oxocarbenium species usually reacts with water, leading to hydrolysis and to the straightforward formation of oxygenated products (Scheme 1a).

Since the discovery of the cumene (**1**) process by Hock and Lang,[1] this reaction has played a crucial role in the production of millions of tons of phenol (**3**) and acetone (**4**) from cumene hydroperoxide (**2**) each year (Scheme 1b).[2] Moreover, this rearrangement has recently been used to produce artemisinin, an antimalarial drug.[3] However, harnessing its potential to develop new synthetic transformations remains a real challenge for organic chemists. Indeed, there have only been limited systematic studies on the selectivity of the Hock cleavage,[4–6] the effect of substituents,[7–9] the catalyst scope[10,11] or synthetic applications.[12–20]

Scheme 1. The Hock rearrangement of organic hydroperoxides: (a) General mechanism; (b) The cumene process; (c) Example of tandem process exploiting the oxocarbenium intermediate.[21]

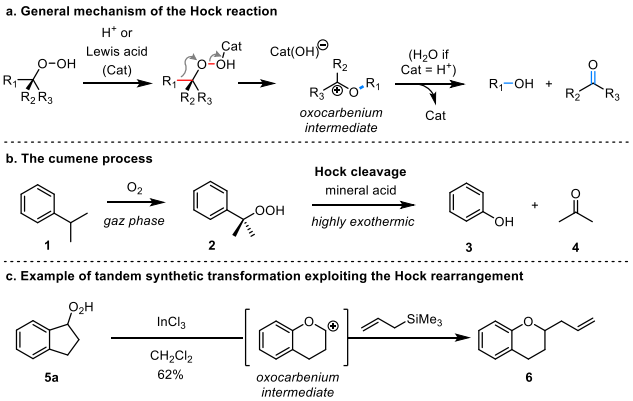

In a joint study, we recently demonstrated the potential of this reaction to synthesize benzoxacycles (*e.g.* chromane **6**) through tandem processes under $InCl_3$ catalysis (Scheme 1c).[21,22] Indeed, by taking advantage of the electrophilic oxocarbenium intermediate generated during the Hock cleavage of indane (*e.g.* **5a**) or tetralin hydroperoxides, the usual hydrolytic process of the reaction could be bypassed by adding nucleophilic species. This work also established that $InCl_3$ is a mild and versatile catalyst to promote the Hock cleavage step.

In spite of this potential, unlike the Baeyer-Villiger rearrangement involving Criegee perester intermediates,[23–29] to the best of our knowledge the Hock reaction has never been theoretically studied. Furthermore, the above-mentioned synthetic work also raises fundamental issues. The relationship between the structure of the hydroperoxide substrate and the efficiency of the reaction remains underinvestigated. The active form of the Lewis acid catalyst $InCl_3$ is another point of interest, as it can potentially act in a monomeric or dimeric form,[30–33] or as a cationic $InCl_2^+$ species,[34] which raises the question of its superelectrophilicity.[35] Herein, we wish to fill these gaps by reporting the first computational study of the Hock rearrangement at the DFT level. The aim was to fully assess this reaction mechanism and thus provide a clear understanding of the observed reactivity. This study also highlights the role and structure of the Lewis acid catalyst $InCl_3$, which has already found numerous applications in organic synthesis.[30–32,36]

RESULTS AND DISCUSSION

In accordance with our recent synthetic work,[37] this theoretical study focuses on the $InCl_3$-catalyzed Hock rearrangement of indane (**5a** and **5b**) and tetralin (**5c** and **5d**) hydroperoxides, leading to chromane and benzoxepane products. Experimental observations[4,37] allow to anticipate several possible reactions from those reactants in presence of a Lewis acid, depending on the coordination site of the catalyst or on the migratory group (Scheme 2). Firstly, during the expected Hock rearrangement from **Ia-d**, two oxocarbenium species could be formed depending on the migration of the sp^2 (giving **IIa-d**, Pathway A) or of the sp^3 carbons (giving **IIIa-d**, Pathway B), respectively resulting in isomeric benzoxacycle derivatives **7a-d** or **8a-d**, the second one being yet never observed in our experiments. Secondly, the elimination of the peroxide group could occur (Pathway C through **IVa-d**), leading to a benzylic carbocation **Va-d** and resulting in alkene **9a-d** upon proton elimination. All these reaction paths have been considered and computationally studied hereafter.

Scheme 2. Anticipation of the outcome of the Hock rearrangement stemming from substrates 5a-d

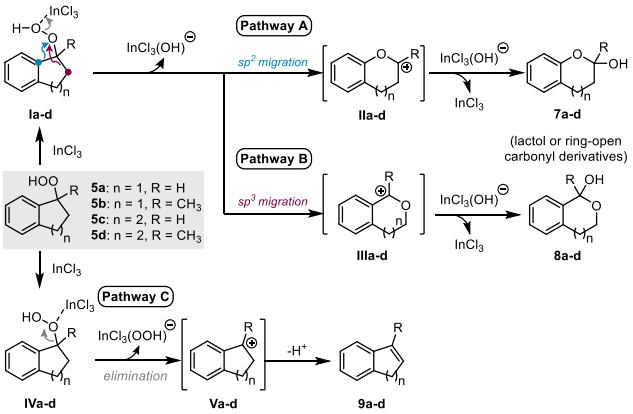

To complement the previous work,[21] an experimental study was performed with substrates **5a-d** to assess their reactivity in presence of $InCl_3$ (Scheme 3). Pathway A shown in Scheme 2, consisting in the migration of the aryl sp^2 carbon, appeared to be predominant for all substrates. Indane peroxides gave lactols **7a/7b**, and dimeric derivatives like 2,2'-oxydichromane **10a** (*anti* isomer, giving suitable crystals for crystallography, Scheme 3) or 2,2'peroxydichromanes **11a/11b** (presence of two diastereoisomers; structure confirmed by HRMS). These two peroxyacetals indicated the release of hydrogen peroxide during the reaction (Scheme 2, Pathway C). However, indene **9a**, an apolar volatile product, was not identified during the isolation process. Conversely, tetralin peroxides afforded acyclic phenolic derivatives **12c** and **12d** (resulting from transient benzoxepane lactols **7c** and **7d**). Neither the regioisomeric isochromanes or 2-benzoxepanes (**8a-d**) resulting from Pathway B or the elimination products (**9a-d**) from Pathway C were observed during this experiment. In the absence of an additional nucleophile, the reaction mixture was however more complex than that of our previous study,[37] probably due to numerous side-reactions occuring on such electrophilic products.

Scheme 3. Experimental study of the Hock rearrangement of indane and tetralin peroxides, and X-ray structure of 10a.

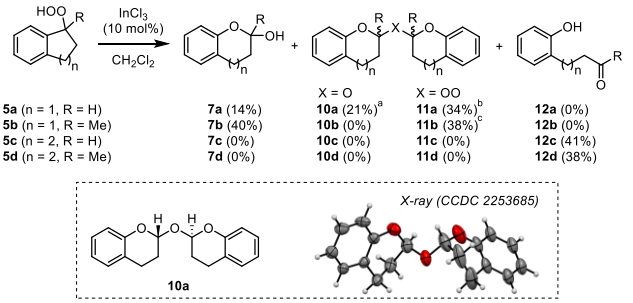

[a] Exclusively isolated as the *anti* diastereoisomer. [b] Two separable diastereoisomers in 20 and 14% yields (undifferentiated). [c] Unseparable diastereomers in a 2:1 ratio.

Our DFT study started with 1-indanyl hydroperoxide **5a** interacting with a single $InCl_3$ molecule (Figure 1). At first, the coordination of $InCl_3$ to the peroxide group provides two potential intermediates, **Ia** and **IVa,** depending on the oxygen involved. Both coordinations are exergonic, respectively by 21.0 and 20.8 kcal/mol. Transition state $\mathbf{TS_{Ia\text{-}IVa}}$, with an energy barrier of ~2.8 kcal/mol, enables easy

interconversion between the two intermediates. We first considered the elimination reaction originating from the coordination of the internal oxygen through intermediate **IVa** (see also Scheme 1, Pathway C). The formation of carbocation **Va** along with $InCl_3(OOH)^-$ is endergonic by 25.5 kcal/mol. Since the dissociation of $InCl_3(OOH)^-$ is more difficult than that of $InCl_3$, this reaction pathway (C) is therefore disfavoured from **5a**, in agreement with the experimental results.

Alternatively, the coordination of $InCl_3$ on the external oxygen of **5a** (**Ia**) can result in two possible intermediates, **VIa** through $\mathbf{TS_{Ia\text{-}VIa}}$ (migration of the adjacent aryl sp^2 carbon) or **VIIa** through $\mathbf{TS_{Ia\text{-}VIIa}}$ (migration of the adjacent alkyl sp^3 carbon). Both transition states involve a Hock rearrangement. However, the energy barrier of $\mathbf{TS_{Ia\text{-}VIa}}$ (referred to as ΔG^{Hock} in Figure 1, blue path) is favored by 9.7 kcal/mol compared to $\mathbf{TS_{Ia\text{-}VIIa}}$, and by 16.7 kcal/mol compared to formation of **Va**. It strongly suggests that only the Hock rearrangement involving the sp^2 carbon can occur, as observed experimentally since the products stemming from $\mathbf{TS_{Ia\text{-}VIa}}$ (**7a**, **10a**, **11a**) were the only one identified (total yield of 69% for the Hock cleavage, Scheme 3).

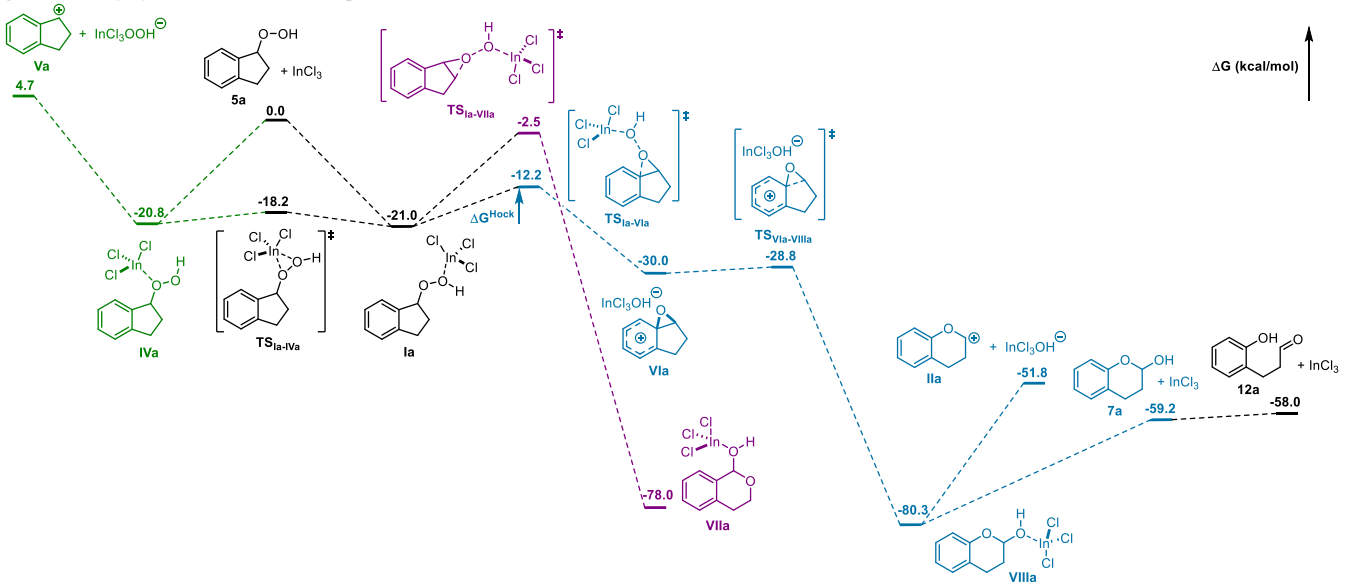

Figure 1. Free-energy profile of the $InCl_3$-catalyzed Hock reaction of 1-indanyl hydroperoxide (**5a**) and other possible secondary reactions.

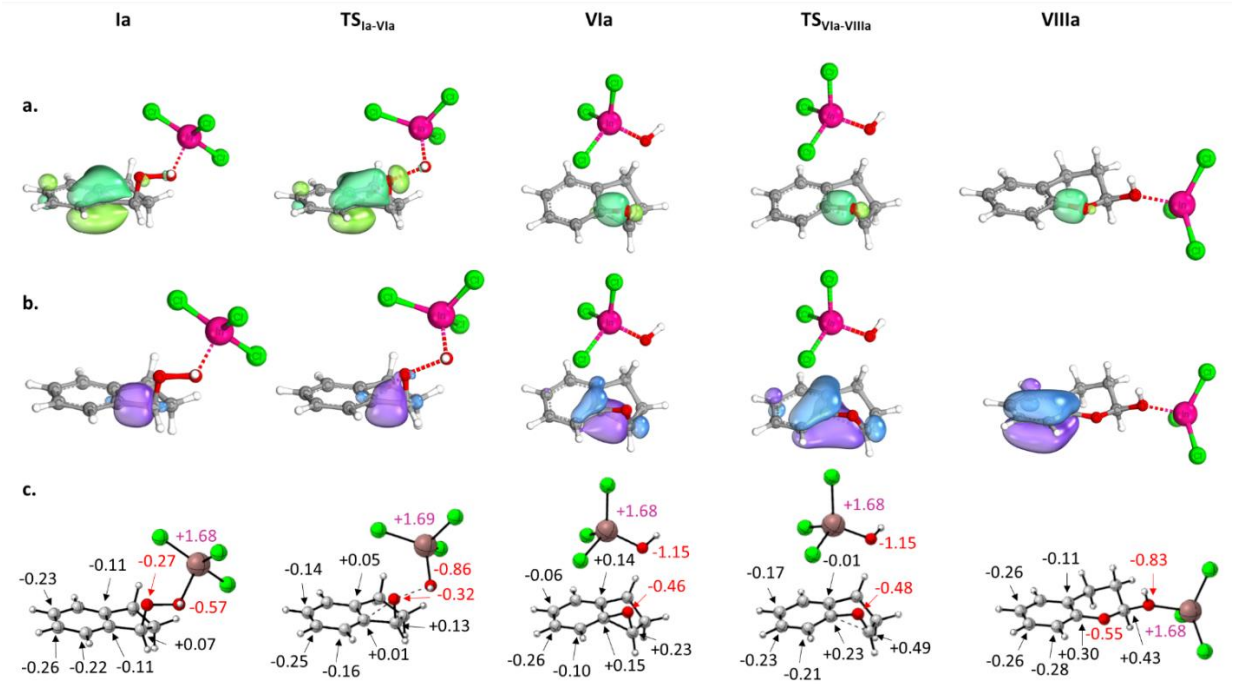

Figure 2. Changes in the electronic structure during the Hock rearrangement. Computation of IBO pathway (a and b) and NBO charges (c) from **Ia** to **VIIIa**.

In fact, this transition state (**TS$_{Ia-VIa}$**) first leads to Wheland intermediate **VIa** (benzenium), which connects to **VIIIa** through **TS$_{VIa-VIIIa}$**. To shed light on the electronic structure changes along this preferred reaction path, the intrinsic bond orbitals (IBO)[38–40] and the atomic charges in the framework of the natural bond orbital[41] (NBO) analyses were computed (Figure 2). IBO enables to visually follow the orbital relocalization during a molecular transformation. It showed that the cleavage occurs with an asynchronous movement of two pairs of electrons. From **Ia** to **VIa**, part of the aryl π cloud is transferred to the closest oxygen of the hydroperoxide (Figure 2a), enabling the formation of the C-O bond and the cleavage of the hydroperoxide O-O bond. From **VIa** to **VIIIa**, the cleavage of the C-C bond is associated with an electronic transfer from this σ-bond back to the aryl group (Figure 2b). Furthermore, NBO analysis underlines the same phenomenon. The charge carried by the benzenium cycle in *ortho* and *para* of the reactive center are less negative in **TS$_{Ia-VIa}$** and **VIa** than in the coordinated compound **Ia**. For example, the charge carried by the *para* carbon passes from –0.23 to –0.06 e, that is a loss of 0.17 e (Figure 2c). Following **TS$_{VIa-VIIIa}$**, formation of **VIIIa** enables the carbon atoms of the aromatic cycle to retrieve their original charge. Notably, the charges carried by the carbon atoms in *meta* are the same along the reaction path, which is consistent with the classical mesomeric forms drawing of the pentadienyl cation moiety of **VIa**.[42] This electron transfer also suggests that the Hock rearrangement is favored by electron-rich aryl rings.

The calculation for *para*-substituted substrates confirmed that π-withdrawing (**5e**, **5f**) and π-donating (**5g**, **5h**) substituents respectively decrease and increase the energy barrier of the Hock rearrangement (ΔG^{Hock}), in good agreement with the electronic density flow analysis during the course of the reaction (Figure 3). Compound **5i**, with a π-donating methoxy group in *ortho,* shows a similar effect as **5h**. In addition, **5j** highlights that the *meta* position has no influence on the barrier of the rearrangement, in good agreement with the above analysis. These results are confirmed by experimental observations regarding the reactivity of substituted substrates[37]: for example, the presence of a strongly π-donating group such as a OMe in *para* position induces an enhanced reactivity of the hydroperoxide substrate which no longer allows its isolation, whereas the reactivity is not modified when the same substituent is in the *meta* position.

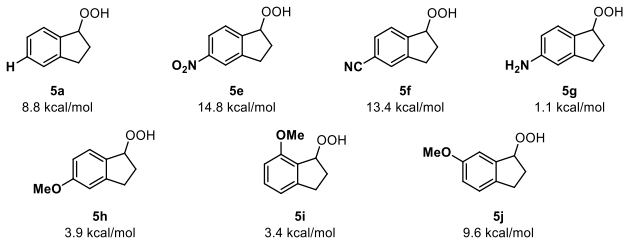

Figure 3. Energy barrier of the Hock rearrangement for substituted substrates (ΔG^{Hock} in kcal/mol).

Stemming from **VIIIa**, the release of $InCl_3(OH)^-$ to form the oxocarbenium species **IIa** is endergonic by 28.5 kcal/mol. However, the release of the catalyst alone from **VIIIa** to generate **7a** is preferred as endergonic by only 21.1 kcal/mol. This energy is close to the energy released by the coordination of $InCl_3$ to the reactant **5a** (21.0 kcal/mol), which suggests close coordination affinities of the catalyst for the starting material and the product. This proximity supports the turnover of catalytic $InCl_3$ and raises the question of the structure of the catalyst (*vide infra*).

To complete this work, the Hock rearrangement of tertiary hydroperoxide **5b** and that of tetralin hydroperoxides **5c** and **5d** was computationally studied, allowing comparison with the previous case (Table 1). Regarding tertiary hydroperoxide **5b**, a better stabilization of benzylic carbocation intermediates **Vb** is expected, favoring a competing elimination of the hydroperoxide over the Hock rearrangement. The formation of the tertiary carbocation **Vb** from **Ib** is easier than that of the secondary one (step **Ia** → **Va**), being endergonic by only 19.3 kcal/mol (25.7 kcal/mol for **Va**). However, the Hock rearrangement remains consistently favored (**TS$_{Ib-VIb}$**), in agreement with experimental results in which no carbocation-derived compound was observed.[37] Furthermore, the Hock reaction is favored by ∼2 kcal/mol (ΔG^{Hock}) when involving a tertiary hydroperoxide rather than a secondary one (Table 1, entry 4). Unlike **5a**, substrate **5b** first led to the formation of oxocarbenium intermediate **IIb**, before hydration leading to **7b** (Table 1, entries 6-7). Similar observations were made for **5c** and **5d**, while these rearrangements did not stop to the lactol products but to the thermodynamically favored open forms **12c** and **12d**, unlike substrate **5a** that led to the more stable lactol **7a**.

Table 1. Free energy of intermediates derived from **5a-d** in the $InCl_3$-catalyzed Hock reaction.

Entry		 **5a**	 **5b**	 **5c**	 **5d**
0	**5**	0.0	0.0	0.0	0.0
1	**IV**	-20.8	-21.7	-28.8	-29.2
2	**V**	4.7	-2.9	0.3	-6.2
3	**I**	-21.0	-22.2	-26.2	-27.2
4	**TS$_{I-VI}$**	-12.2 (8.8)[a]	-15.5 (6.7)[a]	-18.1 (8.6)[a]	-20.8 (6.4)[4]
5	**VIII**	-80.3	-83.1	-80.0	-84.9
6	**II**	-51.8	-62.7	-51.1	-61.3
7	**7**	-59.2	-62.0	-49.7	-52.1
8	**11**	-58.0	-62.2	-56.4	-62.1

[a] The value in parentheses corresponds to ΔG^{Hock}, the energy barrier of the Hock rearrangement in kcal/mol

A final question arose concerning the exact nature of the catalyst. Recent studies showed that the catalytically active species of Lewis acids of type AX_3 (A = Al, Ga, Fe, In and X = H, Cl) are in the dimeric form A_2X_6, or in the form of a superelectrophile like $X_2A\text{-}X\text{-}AX_3$.[33–35,43,44] The Hock rearrangement of **5a** was thus investigated in the presence of dimeric $InCl_3$ (Figure 4**,** not all intermediates are presented, see Supporting information for details).

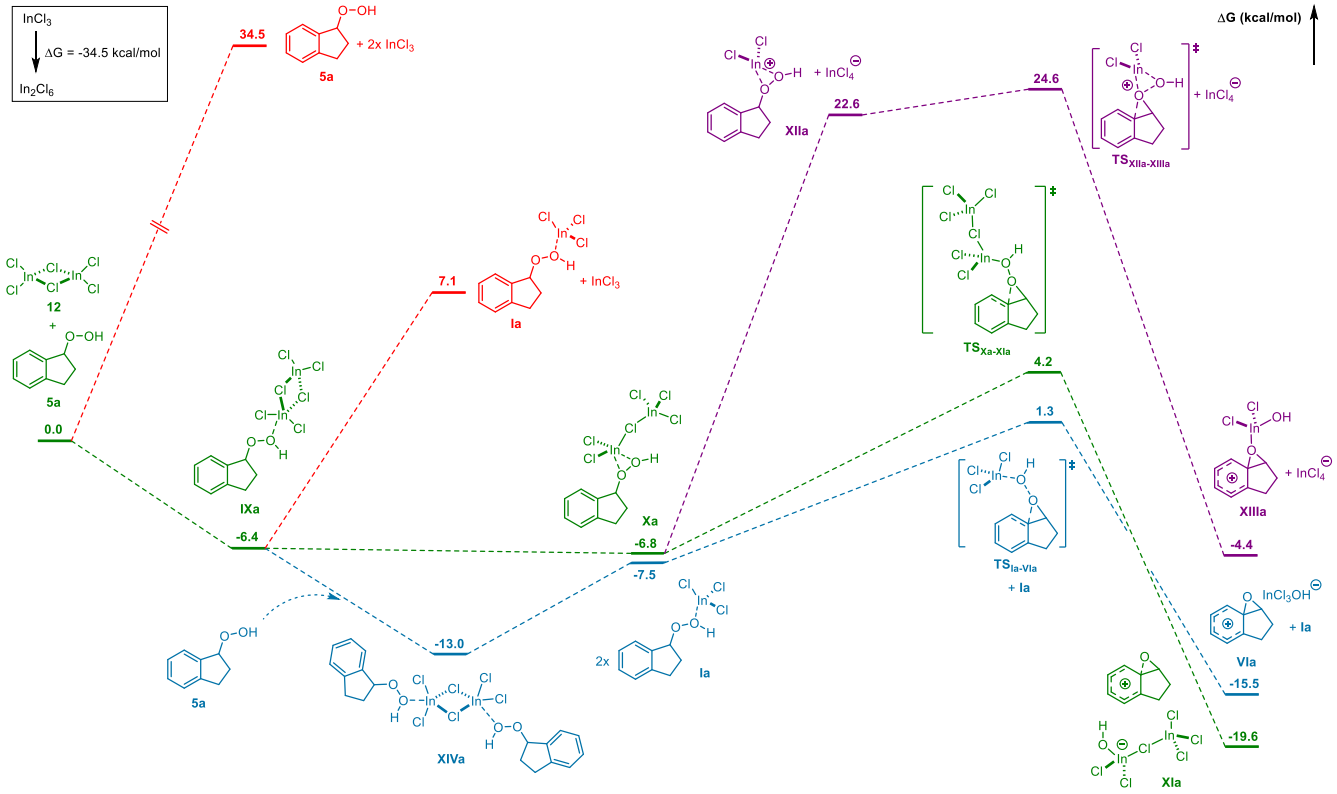

Figure 4. Free-energy profile of the Hock reaction of 1-indanyl hydroperoxide (**5a**) catalyzed by In_2Cl_6 versus $InCl_3$ and $InCl_2^+$.

The dimerization of $InCl_3$ gives rise to a stable homodimer (In_2Cl_6) favored by 34.5 kcal/mol. This dimer is bridged by two chlorin atoms and can coordinate to the peroxide, leading to complex **IXa**. As expected, this coordination is much less exergonic than that of monomeric $InCl_3$ (–6.4 vs –21.0 kcal/mol). Interestingly, **IXa** can reorganize to structure **Xa** bridged by a single chlorin atom between the two indium atoms, thus adopting the Cl_2In-Cl-$InCl_3$ scaffold. Unexpectedly, unlike Ga_2Cl_6 catalysis displaying gallium superelectrophilic species during the reorganization of 1,6 enynes[33] or the methylation of benzene,[44] the dimeric species Cl_2In-Cl-$InCl_3$ is not a superelectrophile able to promote the Hock rearrangement. Indeed, not only **Xa** is not significantly more stable than **IXa** (–0,4 kcal/mol), but more importantly the activating barrier for the Hock rearrangement is in this case higher (+11.0 kcal/mol from **Xa** to $\mathbf{TS_{Xa\text{-}XIa}}$) than with monomeric $InCl_3$ (+8.8 kcal/mol from **Ia** to $\mathbf{TS_{Ia\text{-}VIa}}$). NBO analysis underlines the fact that the In atom coordinated to the hydroperoxide group in **Xa** has a greater positive charge (+1.74 e) than the other In atom (+1.61 e). However, the In-Cl-In bonds show that the Cl atom is closer by 12 pm to the In atom coordinated to the peroxide (Figure 5).

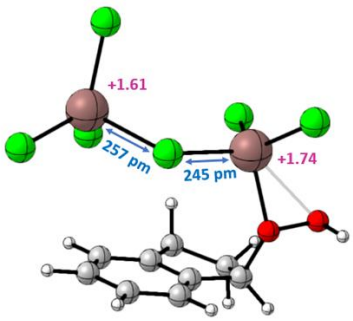

Figure 5: Structure, NBO charges and bond length of intermediate **Xa**.

These structural and electronic differences in the two In atoms of **Xa** do not seem sufficient to allow a representation as [$InCl_2^+$-$InCl_4^-$]. Finally, further calculations demonstrated that $InCl_2^+$ can be a superelectrophilic catalyst for the Hock rearrangement, with an energy barrier reduced to +2.0 kcal/mol from the complex **5a**-$InCl_2^+$ (**XIIa**) to $\mathbf{TS_{XIIa\text{-}XIIIa}}$. However, the high endergonicity of the formation of this complex (+29.4 kcal/mol from **Xa**) precludes any possibility for $InCl_2^+$ to be the catalyst of this reaction.

Finally, we investigated the possible coordination of In_2Cl_6 by two molecules of peroxide substrate (**5a**). It is first interesting to mention that the coordination of an In_2Cl_6 dimer on a single molecule of **5a** (formation of **Xa**: –6.8 kcal/mol) is almost as exergonic as the coordination of two $InCl_3$ monomers on two molecules of **5a** (formation of two **Ia**: –7.5 = +34.5 – 2 x 21.0 kcal/mol). The dissociation of the In_2Cl_6 dimer can neither occur before nor after its coordination to a single molecule of **5a**, because both processes lead to highly energetic intermediates (pathway in red Figure 4). However, a second molecule of **5a** can bind to **IXa**, leading to stable, symmetrical, dimeric intermediate **XIVa** (**5a**·In_2Cl_6·**5a**). This double coordination is consistent with the presence of an excess of substrate **5a** during the reaction. From **XIVa**, two possible pathways can be envisaged: (i) the reversible formation of **IXa** by releasing a molecule of hydroperoxide (endergonic by 6.6 kcal/mol), finally resulting in mono-bridged **Xa**, or (ii) the dissociation of dimeric **XIVa** releasing two molecules of monomeric complex **Ia**, associated to a cost of 5.5 kcal/mol. The latter should thus be the privileged pathway, leading to an $InCl_3$-catalyzed rearrangement through $\mathbf{TS_{Ia\text{-}VIa}}$, endergonic by 8.8 kcal/mol. The direct

In_2Cl_6-mediated Hock rearrangement is more speculative as it goes through **TS$_{Xa\text{-}XIa}$** which is located 2.9 kcal/mol higher than **TS$_{Ia\text{-}VIa}$**.

This study thus points out to monomeric $InCl_3$ as the active catalyst of the rearrangement. It is important to note however that this monomeric catalyst is generated from **XIVa** and only exists in a coordinated form. While $InCl_3$ has a strong and similar affinity for the substrate (**5a**) and the product (**7a**), its tendency to dimerize is even more exergonic. Consequently, free monomeric $InCl_3$ does not exist in solution, while the dimer In_2Cl_6 can be regenerated at the end of the reaction, finally explaining the turnover of this catalyst (Scheme 4).

Scheme 4. Catalytic cycle of the $InCl_3$-catalyzed Hock rearrangement.

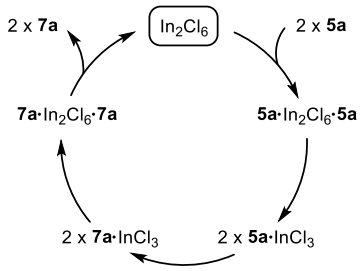

CONCLUSION

In conclusion, this study of the $InCl_3$-catalyzed Hock rearrangement elucidates for the first time the details of the electronic mechanism of this reaction. In particular, the demonstration that a key benzenium intermediate is involved in the reaction gives clues for better stabilization of this intermediate through the choice of appropriate substituents. This benzenium intermediate is a consequence of the migration of the aryl sp^2 *ipso*-carbon onto the internal peroxide oxygen, with concommittant cleavage of the O–O bond. The cleavage of the C–C bond appears to be consecutive to the benzenium formation, highlighting an asynchronous mechanism.

Furthermore, we propose that the catalysis of this reaction (Scheme 4) involves a monomeric complex of $InCl_3$ coordinated to one molecule of hydroperoxide substrate ($InCl_3$·ROOH), originating from the cleavage of the much more stable symmetrical homodimer In_2Cl_6·$(ROOH)_2$. By decreasing the activation barrier of the Hock rearrangement, this coordinated $InCl_3$ monomer behaves as a better electrophile compared to the dimer that is significantly less activating (*e.g.* 8.8 kcal/mol vs. 11.0 kcal/mol for substrate **5a**). Therefore, unlike previous studies highlighting superelectrophilic dimeric species such as A_2X_6 or $AX_2^+AX_4^-$ among the group 13 elements,[33,35,44] our study shows the absence of superelectrophilicity for the dimeric In_2Cl_6 species during this Hock rearrangement. These species are however central in our catalytic cycle, serving as a reservoir of active monomeric catalytic species. Overall, while monomeric species are mostly considered in In(III)-based methodologies, we can reasonably suggest that homodimeric and other coordinated species should be given better attention as part of the catalytic cycle.

COMPUTATIONAL DETAILS

The calculations were performed using Gaussian 09 software. Geometry optimizations and transition states (TS) were obtained employing the 6-31G(d,p) basis set[45,46] on all atoms except for indium which was modeled using LANL2DZ effective core potential and associated double-zeta valence basis,[47] in combination with B3LYP-D3 functional.[48,49] This level of theory previously proved reliable to study the Baeyer-Villiger mechanism.[50] Both TS and geometry optimization were confirmed using frequency calculations at the same level of theory. Solvent effects were included in the calculations thanks to IEFPCM continuum solvation model[51] using dichloromethane as solvent. For every TS found, intrinsic reaction coordinates (IRC)[52,53] were calculated to ensure that the corresponding TS is connected to the proper reactant(s) and product(s). The energy obtained were improved thanks to single point calculation with the same method and aug-cc-pVTZ basis set[54] for all atoms except Indium. Indium was modeled using the multi electron fit fully relativistic effective core potential ECP28MDF[55] in combination with basis set aug-cc-pVTZ-PP. The three-dimensional optimized stuctures were prepared using CYLview20.[56] Intrinsic bond orbitals (IBO) analyses were performed using Iboview software[38–40] on the optimized geometries with default method (PBE/def2-TZVP) to generate Kohn-Sham wave functions. IBO analyses enable to visually follow the movement of electrons during a molecular transformation thanks to the representation of localized molecular orbitals. NBO charges were computed using NBO6 software at the IEFPCM(CH_2Cl_2)-B3LYP-D3/6-31G(d,p) – LanL2DZ level. The Gibbs free energies presented in this article are IEFPCM(CH_2Cl_2)-B3LYP-D3/aug-cc-pVTZ(-PP) //IEFPCM(CH_2Cl_2)-B3LYP-D3/6-31G(d,p) – LanL2DZ electronic energies modified with thermal and entropy corrections from IEFPCM(CH_2Cl_2)-B3LYP-D3/6-31G(d,p) – LanL2DZ calculations. Due to the well-known errors associated with entropy calculations, we apply a scaling factor of 0.5 to the entropic contributions as recommended and successfully used in the literature.[57–61]

ASSOCIATED CONTENT

Supporting Information. Experimental methods, copies of NMR spectra, additional computational details, cartesian coordinates of stationary points and CIF file. The crystallographic data of **10a** have been deposited on the Cambridge Crystallographic Data Center under the CCDC number 2253685. This material is available free of charge via the Internet at http://pubs.acs.org.

AUTHOR INFORMATION

Corresponding Author

* Email addresses for:
Gilles Frison: gilles.frison@cnrs.fr
Bastien Nay: bastien.nay@polytechnique.edu

Author Contributions

The manuscript was written through contributions of all authors.

Funding Sources

Agence Nationale de la Recherche (ANR-19-CE07-0012)
Labex CHARM3AT

ACKNOWLEDGMENT

This work was supporting by the French *Agence Nationale de la Recherche* and by Labex CHARM3AT. The *CNRS*, *l'X, Sorbonne Université* are acknowledged for hosting and funding.

REFERENCES

(1) Hock, H.; Lang, S. Autoxydation von Kohlenwasserstoffen, IX. Mitteil.: Über Peroxyde von Benzol-Derivaten. *Chem. Ber.* **1944**, *77* (3–4), 257–264. https://doi.org/10.1002/cber.19440770321.

(2) Weber, M.; Weber, M.; Weber, V. Phenol. In *Ullmann's Encyclopedia of Industrial Chemistry*; Wiley-VCH Verlag, 2020; pp 1–20. https://doi.org/10.1002/14356007.a19_299.pub3.

(3) Turconi, J.; Griolet, F.; Guevel, R.; Oddon, G.; Villa, R.; Geatti, A.; Hvala, M.; Rossen, K.; Göller, R.; Burgard, A. Semisynthetic Artemisinin, the Chemical Path to Industrial Production. *Org. Process Res. Dev.* **2014**, *18* (3), 417–422. https://doi.org/10.1021/op4003196.

(4) Anderson, G. H.; Smith, J. G. Acid-Catalyzed Rearrangement of Hydroperoxides. II. Phenylcycloalkyl Hydroperoxides. *Can. J. Chem.* **1968**, *46* (9), 1561–1570. https://doi.org/10.1139/v68-256.

(5) Deno, N. C.; Billups, W. E.; Kramer, K. E.; Lastomirsky, R. R. Rearrangement of Aliphatic Primary, Secondary, and Tertiary Alkyl Hydroperoxides in Strong Acid. *J. Org. Chem.* **1970**, *35* (9), 3080–3082. https://doi.org/10.1021/jo00834a046.

(6) Frimer, A. A. The Effect of Strain on the Rearrangement of Allylic Hydroperoxides: A Research Account. *J. Photochem.* **1984**, *25* (2), 211–226. https://doi.org/10.1016/0047-2670(84)87025-2.

(7) Anderson, G. H.; Smith, J. G. Acid-Catalyzed Rearrangement of Hydroperoxides. I. Benzhydryl Hydroperoxides. *Can. J. Chem.* **1968**, *46* (9), 1553–1559. https://doi.org/10.1139/v68-255.

(8) Boger, D. L.; Coleman, R. S. Benzylic Hydroperoxide Rearrangement: Observations on a Viable and Convenient Alternative to the Baeyer-Villiger Rearrangement. *J. Org. Chem.* **1986**, *51* (26), 5436–5439. https://doi.org/10.1021/jo00376a079.

(9) Kabalka, G. W.; Kesavulu Reddy, N.; Narayana, C. Sodium Perborate: A Convenient Reagent for Benzylic Hydroperoxide Rearrangement. *Tetrahedron Lett.* **1993**, *34* (48), 7667–7668. https://doi.org/10.1016/S0040-4039(00)61534-4.

(10) Lange, J.-P.; Breed, A. J. M. Catalytic Rearrangement of an Aliphatic Hydroperoxide. *Catalysis Comm.* **2002**, *3* (1), 25–28. https://doi.org/10.1016/S1566-7367(01)00071-1.

(11) Chaudhari, M. B.; Chaudhary, A.; Kumar, V.; Gnanaprakasam, B. The Rearrangement of Peroxides for the Construction of Fluorophoric 1,4-Benzoxazin-3-One Derivatives. *Org. Lett.* **2019**, *21* (6), 1617–1621. https://doi.org/10.1021/acs.orglett.9b00155.

(12) Boger, D. L.; Coleman, R. S. Further Observations on the Lewis Acid-Catalyzed Benzylic Hydroperoxide Rearrangement: Use of a Boron-Trifluoride/ Hydrogen Peroxide Preformed, Aged Reagent. *Tetrahedron Lett.* **1987**, *28* (10), 1027–1030. https://doi.org/10.1016/S0040-4039(00)95902-1.

(13) Koser, S.; Hoffmann, H. M. R.; Williams, D. J. Stereoselective Synthesis of Precursors of Naturally Occurring Robustadials A and B. *J. Org. Chem.* **1993**, *58* (23), 6163–6165. https://doi.org/10.1021/jo00075a001.

(14) Dussault, P. H.; Lee, H.-J.; Liu, X. Selectivity in Lewis Acid-Mediated Fragmentations of Peroxides and Ozonides: Application to the Synthesis of Alkenes, Homoallyl Ethers, and 1,2-Dioxolanes. *J. Chem. Soc., Perkin Trans. 1* **2000**, No. 17, 3006–3013. https://doi.org/10.1039/B001391I.

(15) Hamann, H.-J.; Liebscher, J. A Novel Outcome of the Hydroperoxide Rearrangement. *J. Org. Chem.* **2000**, *65* (6), 1873–1876. https://doi.org/10.1021/jo991457y.

(16) Hamann, H.-J.; Liebscher, J. Primary Geminal Bishydroperoxides by Hydroperoxide Rearrangement. *Synlett* **2001**, *2001* (01), 0096–0098. https://doi.org/10.1055/s-2001-9704.

(17) Zheng, X.; Lu, S.; Li, Z. The Rearrangement of Tert-Butylperoxides for the Construction of Polysubstituted Furans. *Org. Lett.* **2013**, *15* (21), 5432–5435. https://doi.org/10.1021/ol402509u.

(18) Zielinski, Z. A. M.; Pratt, D. A. Cholesterol Autoxidation Revisited: Debunking the Dogma Associated with the Most Vilified of Lipids. *J. Am. Chem. Soc.* **2016**, *138* (22), 6932–6935. https://doi.org/10.1021/jacs.6b03344.

(19) Laroche, B.; Nay, B. Harnessing the Potential Diversity of Resinic Diterpenes through Visible Light-Induced Sensitized Oxygenation Coupled to Kornblum–DeLaMare and Hock Reactions. *Org. Chem. Front.* **2017**, *4* (12), 2412–2416. https://doi.org/10.1039/C7QO00633K.

(20) Yaremenko, I. A.; Vil', V. A.; Demchuk, D. V.; Terent'ev, A. O. Rearrangements of Organic Peroxides and Related Processes. *Beilstein J. Org. Chem.* **2016**, *12*, 1647–1748. https://doi.org/10.3762/bjoc.12.162.

(21) Bosnidou, A.; Fayet, A.; Cheibas, C.; Gayraud, O.; Bourcier, S.; Frison, G.; Nay, B. Tandem InCl3-Promoted Hydroperoxide Rearrangements and Nucleophilic Additions, a Straightforward Entry to Benzoxacycles. *ChemRxiv* April 4, 2023. https://doi.org/10.26434/chemrxiv-2023-7b93n-v2.

(22) Fayet, A.; Bourcier, S.; Casaretto, N.; Nay, B.; Frison, G. Theoretical Investigation of the Mechanism of the Hock Rearrangement with InCl3 as Catalyst. *ChemRxiv* April 4, 2023. https://doi.org/10.26434/chemrxiv-2023-5hzrp-v3.

(23) Carlqvist, P.; Eklund, R.; Brinck, T. A Theoretical Study of the Uncatalyzed and BF3-Assisted Baeyer–Villiger Reactions. *J. Org. Chem.* **2001**, *66* (4), 1193–1199. https://doi.org/10.1021/jo001278c.

(24) Grein, F.; Chen, A. C.; Edwards, D.; Crudden, C. M. Theoretical and Experimental Studies on the Baeyer–Villiger Oxidation of Ketones and the Effect of α-Halo Substituents. *J. Org. Chem.* **2006**, *71* (3), 861–872. https://doi.org/10.1021/jo0513966.

(25) Alvarez-Idaboy, J. R.; Reyes, L.; Mora-Diez, N. The Mechanism of the Baeyer–Villiger Rearrangement: Quantum Chemistry and TST Study Supported by Experimental Kinetic Data. *Org. Biomol. Chem.* **2007**, *5* (22), 3682–3689. https://doi.org/10.1039/B712608E.

(26) Alvarez-Idaboy, J. R.; Reyes, L. Reinvestigating the Role of Multiple Hydrogen Transfers in Baeyer–Villiger Reactions. *J. Org. Chem.* **2007**, *72* (17), 6580–6583. https://doi.org/10.1021/jo070956t.

(27) Yamabe, S.; Yamazaki, S. The Role of Hydrogen Bonds in Baeyer–Villiger Reactions. *J. Org. Chem.* **2007**, *72* (8), 3031–3041. https://doi.org/10.1021/jo0626562.

(28) Long, Q.; Ji, H.; Lv, S. DFT Study on the Hydrogen Bonds of Phenol–Cyclohexanone and Phenol–H2O2 in the Baeyer–Villiger Oxidation. *Int. J. Quantum Chem.* **2009**, *109* (3), 448–458. https://doi.org/10.1002/qua.21848.

(29) Jin, P.; Zhu, L.; Wei, D.; Tang, M.; Wang, X. A DFT Study on the Mechanisms of Tungsten-Catalyzed Baeyer–Villiger Reaction Using Hydrogen Peroxide as Oxidant. *Comput. Theor. Chem.* **2011**, *966* (1), 207–212. https://doi.org/10.1016/j.comptc.2011.03.002.

(30) Yadav, J. S.; Antony, A.; George, J.; Reddy, B. V. S. Recent Developments in Indium Metal and Its Salts in Organic Synthesis.

Eur. J. Org. Chem. **2010**, *2010* (4), 591–605. https://doi.org/10.1002/ejoc.200900895.
(31) Singh, M. S.; Raghuvanshi, K. Recent Advances in InCl3-Catalyzed One-Pot Organic Synthesis. *Tetrahedron* **2012**, *68* (42), 8683–8697. https://doi.org/10.1016/j.tet.2012.06.099.
(32) Sestelo, J. P.; Sarandeses, L. A.; Martínez, M. M.; Alonso-Marañón, L. Indium(III) as π-Acid Catalyst for the Electrophilic Activation of Carbon–Carbon Unsaturated Systems. *Org. Biomol. Chem.* **2018**, *16* (32), 5733–5747. https://doi.org/10.1039/C8OB01426D.
(33) Yang, S.; Alix, A.; Bour, C.; Gandon, V. Alkynophilicity of Group 13 MX3 Salts: A Theoretical Study. *Inorg. Chem.* **2021**, *60* (8), 5507–5522. https://doi.org/10.1021/acs.inorgchem.0c03302.
(34) Zhuo, L.-G.; Zhang, J.-J.; Yu, Z.-X. DFT and Experimental Exploration of the Mechanism of InCl3-Catalyzed Type II Cycloisomerization of 1,6-Enynes: Identifying InCl2+ as the Catalytic Species and Answering Why Nonconjugated Dienes Are Generated. *J. Org. Chem.* **2012**, *77* (19), 8527–8540. https://doi.org/10.1021/jo301471w.
(35) Olah, G. A.; Klumpp, D. A. *Superelectrophiles and Their Chemistry*; Wiley, 2008.
(36) Mahato, S. K.; Acharya, C.; Wellington, K. W.; Bhattacharjee, P.; Jaisankar, P. InCl3: A Versatile Catalyst for Synthesizing a Broad Spectrum of Heterocycles. *ACS Omega* **2020**, *5* (6), 2503–2519. https://doi.org/10.1021/acsomega.9b03686.
(37) Bosnidou, A. E.; Fayet, A.; Cheibas, C.; Gayraud, O.; Bourcier, S.; Frison, G.; Nay, B. InCl3-Promoted Tandem Hock Rearrangements and Nucleophilic Ad-Ditions, a Straightforward Entry to Benzoxacycles. *submitted* **2023**.
(38) Knizia, G. Intrinsic Atomic Orbitals: An Unbiased Bridge between Quantum Theory and Chemical Concepts. *J. Chem. Theory Comput.* **2013**, *9* (11), 4834–4843. https://doi.org/10.1021/ct400687b.
(39) Knizia, G.; Klein, J. E. M. N. Electron Flow in Reaction Mechanisms—Revealed from First Principles. *Angew. Chem. Int. Ed.* **2015**, *54* (18), 5518–5522. https://doi.org/10.1002/anie.201410637.
(40) Bertus, P. From Dialkyltitanium Species to Titanacyclopropanes: An Ab Initio Study. *Organometallics* **2019**, *38* (21), 4171–4182. https://doi.org/10.1021/acs.organomet.9b00509.
(41) Glendening, E. D.; Landis, C. R.; Weinhold, F. Natural Bond Orbital Methods. *Wiley Interdiscip. Rev. Comput. Mol. Sci.* **2012**, *2* (1), 1–42. https://doi.org/10.1002/wcms.51.
(42) Hadzic, M.; Braïda, B.; Volatron, F. Wheland Intermediates: An Ab Initio Valence Bond Study. *Org. Lett.* **2011**, *13* (8), 1960–1963. https://doi.org/10.1021/ol200327s.
(43) Albright, H.; Riehl, P. S.; McAtee, C. C.; Reid, J. P.; Ludwig, J. R.; Karp, L. A.; Zimmerman, P. M.; Sigman, M. S.; Schindler, C. S. Catalytic Carbonyl-Olefin Metathesis of Aliphatic Ketones: Iron(III) Homo-Dimers as Lewis Acidic Superelectrophiles. *J. Am. Chem. Soc.* **2019**, *141* (4), 1690–1700. https://doi.org/10.1021/jacs.8b11840.
(44) Yang, S.; Bour, C.; Gandon, V. Superelectrophilic Gallium(III) Homodimers in Gallium Chloride-Mediated Methylation of Benzene: A Theoretical Study. *ACS Catal.* **2020**, *10* (5), 3027–3033. https://doi.org/10.1021/acscatal.9b05509.
(45) Francl, M. M.; Pietro, W. J.; Hehre, W. J.; Binkley, J. S.; Gordon, M. S.; DeFrees, D. J.; Pople, J. A. Self-consistent Molecular Orbital Methods. XXIII. A Polarization-type Basis Set for Second-row Elements. *J. Chem. Phys.* **1982**, *77* (7), 3654–3665. https://doi.org/10.1063/1.444267.
(46) Becke, A. D. Density-Functional Exchange-Energy Approximation with Correct Asymptotic Behavior. *Phys. Rev. A* **1988**, *38* (6), 3098–3100. https://doi.org/10.1103/PhysRevA.38.3098.
(47) Chiodo, S.; Russo, N.; Sicilia, E. LANL2DZ Basis Sets Recontracted in the Framework of Density Functional Theory. *J. Chem. Phys.* **2006**, *125* (10), 104107. https://doi.org/10.1063/1.2345197.
(48) Grimme, S.; Antony, J.; Ehrlich, S.; Krieg, H. A Consistent and Accurate Ab Initio Parametrization of Density Functional Dispersion Correction (DFT-D) for the 94 Elements H-Pu. *J. Chem. Phys.* **2010**, *132* (15), 154104. https://doi.org/10.1063/1.3382344.
(49) Grimme, S.; Ehrlich, S.; Goerigk, L. Effect of the Damping Function in Dispersion Corrected Density Functional Theory. *J. Comput. Chem.* **2011**, *32* (7), 1456–1465. https://doi.org/10.1002/jcc.21759.
(50) Li, G.; Fürst, M. J. L. J.; Mansouri, H. R.; Ressmann, A. K.; Ilie, A.; Rudroff, F.; Mihovilovic, M. D.; Fraaije, M. W.; Reetz, M. T. Manipulating the Stereoselectivity of the Thermostable Baeyer–Villiger Monooxygenase TmCHMO by Directed Evolution. *Org. Biomol. Chem.* **2017**, *15* (46), 9824–9829. https://doi.org/10.1039/C7OB02692G.
(51) Scalmani, G.; Frisch, M. J. Continuous Surface Charge Polarizable Continuum Models of Solvation. I. General Formalism. *J. Chem. Phys.* **2010**, *132* (11), 114110. https://doi.org/10.1063/1.3359469.
(52) Fukui, K. Formulation of the Reaction Coordinate. *J. Phys. Chem.* **1970**, *74* (23), 4161–4163. https://doi.org/10.1021/j100717a029.
(53) Fukui, K. The Path of Chemical Reactions - the IRC Approach. *Acc. Chem. Res.* **1981**, *14* (12), 363–368. https://doi.org/10.1021/ar00072a001.
(54) Dunning, T. H. Gaussian Basis Sets for Use in Correlated Molecular Calculations. I. The Atoms Boron through Neon and Hydrogen. *J. Chem. Phys.* **1989**, *90* (2), 1007–1023. https://doi.org/10.1063/1.456153.
(55) Peterson, K. A.; Figgen, D.; Goll, E.; Stoll, H.; Dolg, M. Systematically Convergent Basis Sets with Relativistic Pseudopotentials. II. Small-Core Pseudopotentials and Correlation Consistent Basis Sets for the Post-d Group 16–18 Elements. *J. Chem. Phys.* **2003**, *119* (21), 11113–11123. https://doi.org/10.1063/1.1622924.
(56) Legault, C. Y. *CYLview20, Université de Sherbrooke, 2020*. https://www.cylview.org/ (accessed 2023-03-30).
(57) Cooper, J.; Ziegler, T. A Density Functional Study of SN2 Substitution at Square-Planar Platinum(II) Complexes. *Inorg. Chem.* **2002**, *41* (25), 6614–6622. https://doi.org/10.1021/ic020294k.
(58) Lau, J. K.-C.; Deubel, D. V. Hydrolysis of the Anticancer Drug Cisplatin: Pitfalls in the Interpretation of Quantum Chemical Calculations. *J. Chem. Theory Comput.* **2006**, *2* (1), 103–106. https://doi.org/10.1021/ct050229a.
(59) Li, H.; Lu, G.; Jiang, J.; Huang, F.; Wang, Z.-X. Computational Mechanistic Study on Cp*Ir Complex-Mediated Acceptorless Alcohol Dehydrogenation: Bifunctional Hydrogen Transfer vs β-H Elimination. *Organometallics* **2011**, *30* (8), 2349–2363. https://doi.org/10.1021/om200089m.
(60) Kua, J.; Krizner, H. E.; De Haan, D. O. Thermodynamics and Kinetics of Imidazole Formation from Glyoxal, Methylamine, and Formaldehyde: A Computational Study. *J. Phys. Chem. A* **2011**, *115* (9), 1667–1675. https://doi.org/10.1021/jp111527x.
(61) Pastor, J.; Rezabal, E.; Voituriez, A.; Betzer, J.-F.; Marinetti, A.; Frison, G. Revised Theoretical Model on Enantiocontrol in Phosphoric Acid Catalyzed H-Transfer Hydrogenation of Quinoline. *J. Org. Chem.* **2018**, *83* (5), 2779–2787. https://doi.org/10.1021/acs.joc.7b03248.